ATF4 regulates mitochondrial dysfunction and mitophagy, contributing to corneal endothelial apoptosis in Fuchs' dystrophy.

Saba Qureshi[1], Stefan Y. Kim[1,#], Stephanie Lee[1,#], Lukas Ritzer[1], William Steidl[1], Gayle Joliet Krest[2], Anisha Kasi[1], Varun Kumar[1,3] *

[1]Eye and Vision Research Institute, Department of Ophthalmology, Icahn School of Medicine at Mount Sinai, New York, New York, USA.

[2]Columbia University, New York, USA.

[3]Department of Pharmacological Sciences, Icahn School of Medicine at Mount Sinai, New York, New York, USA.

# These authors have contributed equally to this manuscript.

*Correspondence: Varun Kumar, Icahn School of Medicine at Mount Sinai, 1 Gustave L. Levy Pl, New York, NY 10029, USA; varun.kumar@mssm.edu

Keywords: ATF4, mitochondrial stress, mitophagy, ER stress, cell survival

Abstract:

PURPOSE. Endoplasmic reticulum (ER) stress, mitochondrial dysfunction, and mitophagy are known to contribute independently to corneal endothelial cell (CEnC) apoptosis in Fuchs' endothelial corneal dystrophy (FECD). However, the role of a specific ER stress pathway (PERK-ATF4-CHOP) in regulating these events is unknown. This study aims to investigate the role of ATF4 in regulating mitochondrial dysfunction and mitophagy, which ultimately leads to CEnC apoptosis in FECD.

METHODS. Human corneal endothelial cell line (21T), Fuchs' corneal endothelial cell line (F35T), and primary human corneal endothelial cells were treated with ER stressor tunicamycin (Tun). ATF4 siRNA was used to knock down ATF4 in 21T cell line and primary corneal endothelial cells. Mitophagy and apoptotic proteins were analyzed using Western blotting. *ATF4*$^{+/-}$ and *ATF4* $^{+/+}$ mice were irradiated with UVA to assess ER stress and corneal endothelial apoptosis.

RESULTS. F35T cell line had significantly increased expression of the ER stress pathway as well as caspase-mediated apoptotic molecules compared to 21T at baseline, which further increased after tunicamycin treatment. F35T cells exhibited significantly decreased ATP and MMP, and increased mitochondrial fragmentation, which was further exacerbated after Tunicamycin. F35T cell line also demonstrated inhibition of mitophagy, similar to 21T, after treatment with Tunicamycin, despite the upregulation of mitophagy initiators. ATF4 knockdown attenuated ER and mitochondrial stress proteins, rescued mitochondrial membrane potential (MMP) loss, downregulated mitochondrial fragmentation, activated mitophagy, and prevented cell death under chronic ER stress. *ATF4*$^{+/-}$ mice had increased CE numbers, with improved cellular morphology and decreased ER stress CHOP expression, compared to ATF4+/+ mice post-UVA.

CONCLUSIONS. Pro-apoptotic ATF4 induction following ER stress disrupts mitochondrial function, leading to mitophagy inhibition and CEnC apoptosis. This study highlights the importance of ATF4 in ER-mitochondrial crosstalk and its contribution to CEnC apoptosis in FECD.

27 **INTRODUCTION**

28 Fuchs' endothelial corneal dystrophy (FECD) is a heritable degenerative disorder of the corneal endothelium
29 (CE) that affects about 4% of people over 40 and has a higher incidence in females.[1] The corneal endothelium
30 consists of a single layer of hexagonal cells that line the back surface of the cornea. These cells are essential
31 for maintaining corneal transparency by continuously pumping ions. Proteomic analysis has demonstrated that
32 in FECD, extracellular membrane (ECM) dysregulation leads to aberrant organization of the corneal endothelial
33 layer and Descemet's membrane.[2] The progressive loss of CEnCs, primarily due to apoptosis, is associated
34 with alterations in cellular junctional complexes and the accumulation of extracellular matrix protrusions in
35 Descemet's membrane (DM), known as guttae, which are the key feature of FECD. The molecular pathogenesis
36 of FECD is an area of active research. FECD is the leading cause of corneal transplantation worldwide, with no
37 available pharmacological treatments. Thus, there is an unmet need to understand the disease pathogenesis in
38 order to develop effective pharmacological interventions. Prior work indicates that mitochondrial dysfunction
39 contributes to FECD development.[3,4] Other research has emphasized the importance of ER stress in promoting
40 the pathogenesis of FECD.[5,6] While ER-mitochondrial crosstalk has been shown to play a role in the development
41 of neurodegenerative diseases such as Parkinson's disease, Huntington's disease, amyotrophic lateral
42 sclerosis, and Alzheimer's disease, among others[7-10], there has been significantly less research regarding the
43 role of ER-mitochondrial crosstalk in the development of FECD.

44 Our lab previously demonstrated that ER stress leads to mitochondrial dysfunction and contributes to
45 CEnC apoptosis.[11] Specifically, our lab showed that induction of ER stress in 21T cell line via tunicamycin led to
46 upregulation of three ER stress pathways named PERK-eIF2α-ATF4-CHOP, ATF6, and IRE1α-XBP1[12] along
47 with increased apoptotic proteins. We confirmed that this ER stress induction in the 21T cell line led to decreased
48 ATP production, loss of MMP, and increased mitochondrial fragmentation. While our research showed
49 upregulation of the well-studied PERK-eIF2α-ATF4-CHOP pathway, further research needs to be performed to
50 elucidate the specific role of ATF4 (a major regulatory transcription factor of the PERK-CHOP pathway) in
51 regulating ER-mitochondrial crosstalk and its contribution to FECD pathophysiology.

52 ATF4 is a transcription factor that contributes to the integrated stress response (ISR), which allows
53 eukaryotic cells to maintain homeostasis in response to cellular stresses.[13,14] ATF4 plays a role in cellular

54 homeostatic maintenance and organellar signaling, which may have implications for the mechanistic role of ATF4
55 in ER-mitochondrial crosstalk and the development of FECD, and warrants further investigation. Specifically,
56 ATF4 is upregulated in response to crosstalk between the ER and mitochondria, as research has shown that
57 mitochondrial dysfunction can promote ER stress and, thus, upregulation of the unfolded protein response
58 (UPR), which affects downstream transcription.[15] ATF4 is also a key player in the mitochondrial stress response,
59 as it upregulates cytoprotective genes upon induction of mitochondrial stress.[16] ER-mitochondrial crosstalk has
60 been shown to upregulate mitophagy upon induction of ATF4 by toxic hexavalent chromium.[17] Apart from
61 mitophagy**,** ATF4 facilitates autophagy in the setting of ER stress by transcriptionally regulating proteins that
62 contribute to autophagosome formation.[18] For instance, ATF4 promotes and regulates autophagy in mammalian
63 cells in response to tunicamycin-induced ER stress.[19] In addition to its role in autophagy, ATF4 plays a role in
64 apoptosis by enabling the degradation of the X-linked inhibitor of apoptosis protein (XIAP) during chronic ER
65 stress, thus promoting cell death.[20] Research has demonstrated that ultraviolet (UV) radiation may also play a
66 role in the development of FECD. [21,22] UV radiation can also lead to decreased ATF4 expression, a finding that
67 warrants further investigation.

68 While prior research establishes the role of ATF4 in organellar crosstalk and cellular homeostasis, there
69 is a need for research that examines the mechanistic contribution of ATF4 to FECD pathogenesis. In our lab's
70 previous publication, we discussed the crosstalk between ER and mitochondria in the corneal endothelium. In
71 this paper, we hypothesize that ATF4 plays a crucial role in ER-mitochondrial crosstalk, particularly in
72 mitochondrial stress and mitophagy, which ultimately leads to apoptosis in FECD. This is the first study to
73 demonstrate a differential effect on mitochondrial dysfunction and mitophagy after ER stress induction on normal
74 and Fuchs' corneal endothelial cell lines. This study specifically investigates the role of ATF4 in mitochondrial
75 stress and apoptosis and Parkin-mediated mitophagy. Finally, this study examines the effect of genetic loss of
76 ATF4 on CE cell viability after an Ultraviolet A (UVA)-induced FECD model *in vivo*.

77 **METHODS**

78 **Normal and Fuchs' cell line culture**

79 Human corneal endothelial cell line (21T) (a kind gift from Ula V. Jurkunas, Harvard University) was maintained
80 in Chen's medium containing Opti-MEM (cat no. 51985034; Thermo Fisher, Waltham, MA, USA), 8% fetal bovine

81 serum (cat no. A3840002; Thermo Fisher), 0.1 gm calcium chloride (cat no. C7902; Sigma-Aldrich, St. Louis,
82 MO, USA), 0.4 gm chondroitin sulfate (cat no. C9819, Sigma Aldrich), gentamycin (0.5%) (cat no. 15750078;
83 Thermo Fisher) antibiotic-antimycotic (1%) (cat no. 15240096; Millipore Sigma, Burlington, MA, USA), 25 µL of
84 epidermal growth factor (cat no. GF144; Thermo Fisher) 50 µg of bovine pituitary extract (cat no. 50-753-3049;
85 Fisher Scientific). Cells were grown on a T75 flask (cat no. 156499; Thermo Fisher) coated with FNC coating
86 mix (cat no. 0407; Athena Enzyme Systems, Baltimore, MD, USA) passaged every two or three days and
87 maintained in an incubator containing 5% CO2 at 37°C. The culture of Fuchs' corneal endothelial dystrophy cell
88 line 35 (F35T, 1500 CUG repeats) (a generous gift from Dr. Albert S. Jun, Johns Hopkins University) was
89 maintained in Opti-MEM (cat no. 51985034; Thermo Fisher) supplemented with 8% fetal bovine serum, 0.1 gm
90 calcium chloride (cat no. C7902; Sigma-Aldrich), 0.4 gm chondroitin sulfate (cat no. C9819; Sigma-Aldrich),
91 gentamycin (0.5%) (cat no. 15750078; Thermo Fisher), antibiotic-antimycotic (1%) (cat no. 15240096; Millipore
92 Sigma), 25 µL of epidermal growth factor (cat no. GF144; Thermo Fisher), 100 µL of nerve growth factor (cat no.
93 13257-019; Thermo Fisher), and 10 mg of ascorbic acid (cat no. 255564; Sigma-Aldrich). Cells were grown on
94 a T25 flask (cat no. 156340; Thermo Fisher) coated with FNC coating mix (cat no. 0407; Athena Enzyme
95 Systems), passaged every two or three days, and maintained in an incubator containing 5% CO_2 at 37°C.

96 **Human primary corneal endothelial culture**

97 We isolated corneal endothelial cells from human donor corneal tissues (Eversight, Chicago, IL, USA) and
98 established primary cell culture. Corneas were washed with M199 medium (Gibco) supplemented with
99 gentamycin (0.5%) and antibiotic-antimycotic (1%). The corneal endothelium layer was peeled off from
100 Descemet's membrane (DM), stripped into smaller pieces, and placed in a tube with fetal bovine serum (15%),
101 antibiotic-antimycotic (1%), gentamycin (0.5%) and it was incubated for 2-5 days. It was then centrifuged at 3000
102 rpm for 6 min at RT, the supernatant was discarded, and the cells/DM strips were rinsed with HBSS by gentle
103 flicking, re-pelleted, added 0.02% EDTA, and incubated at 37°C for 1 h. Then the tissue/cells were passed
104 through a glass Pasteur pipette 15-20 times gently and added 2 ml of growth medium and centrifuged at 3000
105 rpm for 6 min at RT, supernatant was discarded, and pellet was resuspended in 500 µL of growth medium. The
106 primary cell culture was maintained in growth medium constituted of Opti-MEM-1 (Gibco) supplemented with 8%
107 FBS, 5 ng/ml human recombinant EGF (Peprotech), 20 ng/ml human recombinant NGF (Peprotech), 100 µg/ml
108 bovine pituitary extract (Biomedical tech), 0.5 mM Ascorbic acid 2-phosphate (Sigma), 200 mg/L $CaCl_2$, 0.08%

109 chondroitin sulphate, 0.5% gentamycin, 1% antibiotic-antimycotic, passaged every 2 days and maintained in an
110 incubator containing 5% CO_2 at 37°C.

111 **siRNA transfection**

112 21T, F35T, and primary corneal endothelial cells were transfected with silencer-select negative control siRNA
113 (cat no. 4390846) or ATF4 siRNA (cat no. 4392420), (both Thermo Fisher Scientific, CA, USA) by using a
114 Lipofectamine RNAi Max transfection reagent (Invitrogen, Life Technologies, CA, USA) according to
115 manufacturer's protocol. At 48 h after transfection, the cells were subjected to different doses of tunicamycin
116 based on the needs of the different experiments.

117 **MTT assay for cell viability**

118 The primary corneal endothelial cells (1×10^4 cells/well) were seeded and grown in 96-well plates (cat no.
119 701003; Fisher Scientific). Cells were transfected with ATF4 siRNA and then treated with dimethyl sulfoxide
120 (DMSO) (0.2%) and tunicamycin (10 μg/mL) and incubated for 24 hours. We performed MTT (3-(4,5-
121 dimethylthiazol-2-yl)-2-5-diphenyltetrazolium bromide) assay (cat no. V13154; Thermo Fisher) for determining
122 cell viability after different tunicamycin treatments as per the manufacturer's protocol.

123 **Measurement of MMP**

124 MMP was measured using the TMRE-Mitochondrial Membrane Potential Assay Kit (ab113852; Abcam) as per
125 the manufacturer's protocol. 21T and F35T (1×10^4 cells/well) cells were seeded in 96-black well flat bottom
126 plates (cat no. 3916; Corning, Inc., Corning, NY, USA) until 70% to 80% confluency, then treated with and without
127 different concentrations of tunicamycin (0.01, 0.1, 1 and 10 μg/mL) and then incubated for 48 hours. Then,
128 fluorescence (ex/em: 549/575 nm) was measured using a plate reader (Varioskan LUX; Thermo Fisher). We also
129 transfected primary corneal endothelial cells with ATF4 siRNA for ATF4 knockdown and assessed MMP.

130 **Measurement of Complex V (ATP Synthase) activity for ATP production**

131 21T cells were seeded in 150 mm plates until 70-80% confluent, and corresponding treatments were applied to
132 the cells for 48 hours. Post-treatment, cells were pelleted, and sample preparation, along with measurement of
133 Complex V activity, was performed using the ATP Synthase Enzyme Activity Microplate Assay Kit as per

134 manufacturer's protocol (cat no. ab109714; Abcam, Cambridge, UK). Absorbance was measured at OD 340 nm
135 at 30°C using a microplate reader (Varioskan LUX; Thermo Fisher).

136 **Caspase 3/7 assay**

137 21T and F35 cells (1 x 10^4 cells/well) were seeded in white walled 96-well plates, until 70% confluency. The
138 cells were then treated with DMSO (0.2%) or tunicamycin (10 µg/ml) and incubated for 24 hours. After incubation,
139 cells were treated with Caspase-Glo 3/7 reagent (G8090, Promega) according to manufacturer protocol. Then
140 the luminescence was measured using a plate reader (Varioskan LUX; Thermo Fisher).

141 **Transmission Electron Microscopy**

142 21T and F35T (4×10^4 cells/well) were seeded in 8 well Permanox Lab-Tek Chamber Slides (cat no. 70413;
143 Fisher Scientific), grown to 80% confluency, and treated with 10 µg/mL of tunicamycin. For the transfection
144 experiment, HCEnC-21T was transfected with negative control siRNA or ATF4 siRNA and then treated with 10
145 µg/mL of tunicamycin. Cells were fixed with 2% paraformaldehyde/2.5% glutaraldehyde in 0.1M sodium
146 cacodylate solution (cat no. 15960-01, Electron Microscopy Sciences (EMS); Fisher Scientific) at 4°C, rinsed in
147 0.1 M sodium cacodylate buffer, then post-fixed with 2% osmium tetroxide/1.5% potassium ferricyanide in 0.1 M
148 sodium cacodylate, and en bloc stained with 2% uranyl acetate in dH2O. Cells were dehydrated in an ethanol
149 series (25% EtOH/dH2O up to 100% EtOH), infiltrated through an ascending ethanol/resin series (cat no. 14120,
150 EMS Embed 812 Kit; Fisher Scientific) and placed in pure resin overnight. Chambers were separated from the
151 slides, and a modified BEEM embedding capsule (EMS, cat no. 70000-B; Fisher Scientific) was placed over
152 defined areas containing cells. Capsules were filled with a drop of pure resin and placed in a vacuum oven to
153 polymerize at 60°C for several hours. Epon resin was added to fill the capsules and polymerized for 72 hours in
154 the vacuum oven. Immediately after polymerization, capsules were snapped from the substrate with pliers to
155 dislodge the cells from the slide. Semithin sections (0.5 µm) were obtained using a Leica UC7 ultramicrotome
156 (Leica), counterstained with 1% toluidine Blue, placed under a coverslip, and viewed under a light microscope
157 to identify successful dislodging of cells. Ultra-thin sections were collected on copper 300 mesh grids using a
158 Coat-Quick adhesive pen. Sections were counter-stained with 1% uranyl acetate and lead citrate and imaged
159 on an HT7500 transmission electron microscope (Hitachi HighTechnologies, Tokyo, Japan) using an AMT
160 NanoSprint12 12- megapixel CMOS transmission electron microscopy (TEM) Camera (Advanced Microscopy

161 Techniques, Danvers, MA, USA). Final images (20–30 images per condition) were collected, and the brightness,
162 contrast, and size of these images were adjusted using Adobe Photoshop CS4 software version CS4 11.0.1
163 (Adobe, Inc., San Jose, CA, USA).

164 **Parkin plasmid transfection**

165 21T cells were transfected with 0.4 µg of YFP-Parkin using Lipofectamine RNAi Max transfection reagent
166 (Invitrogen, Life Technologies, CA, USA) and incubated for 30 hours. Then, we added DMSO and tunicamycin
167 (20 µg/mL) for 6 hours. The cells were then fixed in PFA, permeabilized in PBS and Triton X, and blocked for 1
168 hour (normal goat serum+ 0.1 g BSA+ Tween 20). Then we incubated with mouse anti-Cytochrome C (cat
169 no.12963S, 1:1000; Cell Signaling) overnight at 4°C. The next day, the cells were incubated with goat anti-mouse
170 secondary antibody (Alexa Fluor 647, cat no. 1510115 1:1000; Abcam) for 1 hour. Cells were washed with PBS,
171 stained with DAPI, and visualized on a confocal microscope.

172 **Immunostaining**

173 21T (4×10^4 cells/well) and F35T were seeded in 2, 4 or 8 well chamber slides to grow up to 70% to 80%
174 confluency. For ATF4/Mitotracker staining, the cells were incubated with MitoTracker Deep Red FM (50 nM) (cat
175 no. M22426; Invitrogen) for 30 minutes, then fixed with paraformaldehyde (PFA) (4%) (cat no. J19943.K2;
176 Thermo Fisher) for 20 minutes, blocked for one hour in blocking buffer (5% normal goat serum + 0.3% Triton X-
177 100 [cat no. X100; Millipore Sigma]) and then incubated with rabbit anti- ATF4 antibody (cat no. 11815S, 1:1000;
178 Cell Signaling, Danvers, MA, USA) overnight at 4°C. The next day, the cells were washed with ice-cold phosphate
179 buffer saline solution (PBS) (cat no. 10010072; Thermo Fisher) three times and incubated with goat anti-rabbit
180 secondary antibody (Alexa Fluor 488, cat no. ab1550077, 1:1000; Abcam, Cambridge, UK) for 1 hour. Cells were
181 washed again with cold-ice PBS and stained nuclei with DAPI (cat no. D1306; Invitrogen). Slides were visualized
182 on a confocal microscope (Leica STED 3X; Leica, Wetzlar, Germany). We also used primary corneal endothelial
183 cells to probe for cytochrome C and ATF4. A similar immunocytochemistry method was used for staining
184 mitochondria by mouse anti-cytochrome C (cat no. 12963S, 1:1000; Cell Signaling) and co-incubated with rabbit
185 anti- ATF4 antibody except for treatment (0.4% DMSO; 10 µg/mL Tun, 24 hours) prior to fixation. The next day,
186 the cells were co-incubated with goat anti-rabbit secondary antibody (Alexa Fluor 488, cat no. ab1550077) and
187 goat anti-mouse secondary antibody (Alexa Fluor 647, cat no. ab1510115, 1:1000; Abcam) for 1 hour. Cells were

188 washed with PBS and stained with DAPI and visualized on a confocal microscope. For transfection experiment,
189 primary corneal endothelial cells were transfected with negative control siRNA or ATF4 siRNA. At 48 h after
190 transfection, the cells were treated with 10 μg/mL of tunicamycin for 24 hours, then followed the same staining
191 procedure for ATF4 and cytochrome C. For the human corneal tissue immunostaining, Descemet's membrane
192 containing endothelial cells was stripped from human donor corneas and treated with DMSO (0.2%) and
193 tunicamycin (10 μg/mL) and incubated for 24 hours. After treatment, fixation, and blocking, the tissues were then
194 incubated with mouse anti-CHOP antibody (cat no. 2895S, 1:1000; Cell Signaling) and rabbit anti-ATF4 antibody
195 overnight at 4°C. For quantifying $ATF4^{+}DAPI^{+}$ cells per visual field (×40 lens), 10 to 15 images were taken under
196 each condition, and the total number of $ATF4^{+}$ $DAPI^{+}$ cells (25-30) was counted and averaged. A similar
197 procedure was followed for calculating the percentage of fragmented mitochondria using cytochrome C.
198 Quantification was masked to reduce the experimental bias. For ZO-1 staining, a dissected mouse cornea cup
199 was fixed with 70% ethanol for 30 min at room temperature, permeabilized with 0.2% Triton X-100 in PBS for 10
200 min, and then blocked with 2% bovine serum albumin (BSA)-PBS for 15 to 30 min. The cornea cup was then
201 incubated with the mouse anti-CHOP antibody (1:400, Cell Signaling) for CHOP immunostaining assay or an
202 anti-ZO-1 antibody (cat no. ZO1-1A12, Invitrogen) for ZO-1 assay in 4% BSA-PBS at 4 °C overnight. The tissues
203 were washed with PBS the following day and incubated with goat anti-mouse secondary antibody for 1 hour.
204 Slides were made and imaged with confocal microscopy. In vivo CE quantification was performed using ImageJ
205 software with the Cell Counter function to count stained cells within each visual frame. For each experimental
206 condition, five images were analyzed, and cell counts from these images were averaged to obtain a
207 representative cell count.

208 **Western blot**

209 21T and F35T were treated either with or without DMSO or tunicamycin (DMSO: 0.0002, 0.002, 0.02, 0.2%;
210 tunicamycin: 0.01, 0.1, 1, 10 μg/mL) for 24 hours for analyzing ER and mitochondrial stress proteins. Primary
211 corneal endothelial cells were transfected with ATF4 siRNA and treated with DMSO or tunicamycin (10 μg/mL)
212 for 24 hours for analyzing autophagy markers. Cells were lysed using RIPA lysis and extraction buffer (cat no.
213 89900; Thermo Fisher) containing protease and phosphatase inhibitor cocktail (cat no. 78440, 1:1000; Thermo
214 Fisher) at 24 hours and spun in a centrifuge at 10,000g for 10 minutes at 4°C. The supernatant was collected
215 and assessed to quantify protein concentration (A53227; Thermo Fisher). For the transfection experiment,

primary corneal endothelial cells were transfected with negative control siRNA or ATF4 siRNA. At 48 h after transfection, the cells were treated with 10 μg/mL of tunicamycin. Protein 30 μg mixed with appropriate LDS sample buffer (cat no. NP0007; Thermo Fisher) and reducing agent (cat no. NP0009; Thermo Fisher) was subjected to 4% to 12% sodium dodecyl sulfate-polyacrylamide gel electrophoresis (cat no. NP032; Thermo Fisher), followed by transfer to polyvinylidene difluoride membrane (cat no. 88518; Thermo Fisher) at 30 V for 90 minutes. The blots were blocked in blocking buffer (25 mM Tris, 0.15 M NaCl, 0.05% Tween 20, 5% skim milk) for one hour at room temperature and then treated with primary antibody (p-eIF2α cat no. 3597, eIF2α cat no. 5324, CHOP cat no. 2895, ATF4 cat no. 11815, GAPDH cat no. 97166, Bcl2 cat no. 4223, cleaved caspase 9 cat no. 20750, cleaved caspase 3 cat no. 9661, PARP cat no. 9532, Mfn2 cat no. 11925, PINK1 cat no. 6946, Parkin cat no. 4211, LC3A/B cat no. 12741, Tim23 cat no. 67535, LC3B cat no. 3868, VDAC cat no. 4661, P-mTOR cat no. 5536, mTOR cat no. 2983, P-Akt cat no. 4060, Akt cat no. 4691, P-AMPKα cat no. 2535, AMPKα cat no. 5831, Actin cat no. 3700; all from Cell Signaling; except Tim23 from Proteintech) overnight at 4°C. The next day, the blots were washed three to five times in TBS-Tween 20 (25 mM Tris, 0.15 M NaCl, 0.05% Tween 20) (cat no. 28360; Thermo Fisher) and HRP-conjugated secondary antibody (anti-mouse IgG cat no. 7076S, Anti-rabbit IgG cat no. 7074S; Cell Signaling) was added for one hour with similar subsequent washing. The immunoreactive bands were visualized using a Femto (cat no. 34094; Thermo Fisher) or pico chemiluminescent substrate (cat no. 34579; Thermo Fisher). The band intensity was measured and quantified using ImageJ software.

Animals

ATF4$^{+/+}$*, ATF4*$^{+/-}$*,* mice (JAX:013072) were generated at Jackson Laboratory (Farmington, CT, USA) by embryo reconstitution and crossing with healthy wild-type-C57BL6/N mice. Monogamous pairs consisting of one male and one female ATF4+/+ and ATF4+/- mouse were crossed as per a homozygous X heterozygous breeding scheme. Litters were genotyped by TransnetYX (Cordova, TN) to identify *ATF4*$^{+/+}$ and *ATF4*$^{+/-}$ mice. Mice were housed at the Animal Housing Facility, Eye and Vision Research Institute (EVRI), Mount Sinai, New York, USA, in a controlled environment with a constant temperature, a 12-h light/dark cycle, and food and water available ad libitum. Mice were anesthetized with a combined dose of ketamine (100 mg/kg) and xylazine (20 mg/kg) administered intraperitoneally (IP). Animal studies were in accordance with the ARVO Statement for the Use of

243 Animals in Ophthalmic and Visual Research as well as the NIH Guide for the Care and Use of Animals and were
244 performed at EVRI with approval from EVRI Institutional Animal Care and Use Committees IACUC.

245 **UVA irradiation**

246 The methods of UVA irradiation of mouse cornea were described in our earlier publication. Briefly, we created a
247 UVA LED light source (M365LP1; Thorlabs, USA) with an emission peak of 365 nm light, 8 nm bandwidth
248 (FWHM). The irradiance of 398 mW/cm^2 was focused down to a 4 mm diameter illumination spot onto the mouse
249 cornea. The time of UVA exposure was adjusted to deliver the appropriate fluence (23 minutes for 200 J/cm^2) as
250 measured with a thermal power sensor head (S425C, Thorlabs, USA) and energy meter console (PM100D,
251 Thorlabs). We irradiated the right eye (OD) with UVA, while the contralateral eye (OS) served as an untreated
252 control and was covered with retention drapes (SpaceDrapes, Inc., USA). Mouse eyes were enucleated in sterile
253 PBS, and corneas containing Descemet's membrane were isolated and immunostained based on experiments.
254 We have considered sacrificing mice on day 1 and week 4 post-UVA for counting CEnC numbers and ER stress
255 marker protein, CHOP, respectively.

256 **RESULTS**

257 **Differential activation of ER stress pathway, PERK-eIF2α-ATF4-CHOP, after chronic ER stress in 21T and**
258 **F35T cell lines, primary CE culture, and human corneal tissues**

259 Previous studies have observed morphological changes in the ER along with increased expression of eIF2 and
260 CHOP proteins of PERK-eIF2α-ATF4-CHOP ER stress pathway within the corneal endothelium of FECD
261 patients.[23] Thus, we first investigated whether there is differential activation of ER stress-related proteins in the
262 PERK-eIF2α-ATF4-CHOP pathway, specifically eIF2α, p-eIF2α, ATF4, and CHOP proteins, in F35T and 21T cell
263 lines after Tun-induced chronic ER stress. Western blotting data showed increased expression of peIF2α, ATF4,
264 and CHOP in F35T compared to the 21T after Tunicamycin (Tun). **(Fig.1A, B)**. Our primary focus was on pro-
265 apoptotic ATF4 and CHOP proteins in this study. Immunostaining data showed a significant induction of ATF4
266 (mainly in the nucleus, with some induction in mitochondria) in F35T compared to 21T cell line under normal
267 physiological conditions **(Fig. 1C, D).** This is confirmed by our previous publication, in which we observed
268 baseline activation of the PERK-EIF2α-ATF4-CHOP pathway proteins in the F35T compared to the 21T.[12] We
269 also investigated this by using primary endothelial cells derived from human corneal tissues. We observed

270 increased ATF4 expression after Tun treatment compared to DMSO in primary endothelial cells **(Fig. 1E)**. To
271 further validate these data, we used corneal tissues and investigated ATF4 and CHOP expression after Tun
272 treatment. We demonstrated increased expression of ATF4 and CHOP proteins after treatment with Tun
273 compared to DMSO in human corneal tissue (specifically CEnCs) using immunohistochemistry **(Fig. 1F)**. These
274 data suggest the potential involvement of the PERK-eIF2α-CHOP ER stress pathway in the pathogenesis of
275 FECD.

276 **Differential mitochondrial dysfunction and apoptosis induced by chronic ER stress in 21T and F35T cell**
277 **lines**

278 ER stress is known to induce mitochondrial stress and dysfunction by initiating the loss of MMP, decreased ATP
279 production, and subsequent release of cytochrome C from the mitochondria.[12] We first investigated whether
280 there are any baseline differences in MMP between normal and Fuchs' cell lines. There were no differences in
281 MMP for 21T and F35T cell lines at baseline. However, when we induced ER stress using tun, we observed a
282 dose-dependent decrease in MMP with Tun in F35T compared to 21T cell lines (**Fig. 2A**). We also found a
283 significantly decreased ATP production in F35T compared to 21T cell line at a basal level which further attenuated
284 after treatment with Tun **(Fig. 2B)**. Immunostaining data also showed increased mitochondrial fragmentation in
285 F35T cell line compared to 21T cell line under DMSO control which further increased after Tun-induced ER stress
286 **(Fig. 2C, D)**. These data suggest that Fuchs cells exhibit higher mitochondrial damage compared to control cells
287 under chronic ER stress. We further investigated whether mitochondrial dysfunction leads to apoptosis. Western
288 blot and quantification data showed upregulation of PARP, cleaved caspase 3 and 9, as well as downregulation
289 of Bcl-2 in F35T compared to 21T cell line at baseline **(Fig. 2E, F).** Next, we performed a cleaved caspase 3/7
290 assay and found a significant increase in cleaved caspase 3/7 activity in F35 compared to 21T under Tun **(Fig.**
291 **2G)**. Furthermore, we also found an increased trend in cleaved caspase 3 protein expression and no significant
292 differences in Bcl-2 between F35 and 21T under Tun (**Fig. 2H**). We also found a significant increase in cleaved
293 PARP (**Fig. 2I**) and caspase 9 **(Fig. 2J)** in F35 compared to 21T under Tun. These data suggest increased
294 caspase-mediated apoptosis in Fuchs compared to control under chronic ER stress, possibly contributed by
295 mitochondrial dysfunction.

296 **Mitophagy activation under chronic ER stress in 21T and F35T cell lines**

297 We hypothesized that mitochondrial dysfunction plays a crucial role in initiating mitophagy events. Thus, we
298 determined the expression of a major mitophagy-contributing protein/mitochondrial fusion protein, mitofusin 2
299 (Mfn2), and mitophagy initiator proteins (PINK1, Parkin, LC3II/I) in F35T and 21T after chronic ER stress. We
300 found a significant upregulation of Parkin and LC3, but a downregulation of PINK1 and Mfn2 in F35T compared
301 to 21T at baseline **(Fig. 3A, B**). Mfn2 was further attenuated in both 21T and F35T cell lines after Tun **(Fig. 3C,**
302 **D)**. Moreover, LC3II/I, specifically LCII denoted by the lower band **(Fig. 3C, D)** and Parkin **(Fig. 3E, F)**,
303 significantly increased in both F35T and 21T after Tun treatment. However, there was a downregulation of PINK1
304 in both F35T and 21T cell lines after Tun **(Fig. G, H).** These data suggest that the initial steps in mitophagy are
305 already activated at baseline in the Fuchs cell line, requiring no further activation of mitophagy initiator proteins
306 (Parkin, LC3) and downregulation of the mitophagy contributor protein (Mfn2). To confirm Parkin-mediated
307 mitophagy activation under chronic ER stress, we transfected 21T with YFP-Parkin and found a significant
308 increase in Parkin localization in the fragmented mitochondria of 21T after Tun **(Fig. 3I, J)**. Although Parkin-
309 mediated mitophagy initiation is reported in Fuchs. However, it is unknown in Fuchs whether the mitophagy
310 process is completed, resulting in fewer mitophagosomes containing damaged mitochondria. This is more
311 relevant here since in cardiac[24] and skeletal diseases[25], loss of Mfn2 is associated with the inhibition of
312 mitophagy, resulting in increased mitophagosomes containing damaged mitochondria. Our TEM data suggest
313 an increase in mitophagosomes in F35 and 21T cells after Tun treatment (**Fig. 3K),** indicating inhibition of
314 mitophagy in both cell lines and no differences in mitophagy regulation following chronic ER stress. This
315 contrasted with the activation of mitophagy initiators in both cell lines after chronic ER stress (**Fig. 3C-F**).

316 **ATF4 knockdown decreases pro-apoptotic ER and mitophagy mediator proteins, attenuates**
317 **mitochondrial fragmentation and MMP loss, and increases cell viability under chronic ER stress**

318 As described earlier, ATF4 is a transcription factor that is activated in response to chronic ER stress in many
319 diseases.[26,27] To investigate the role of ATF4 in regulating ER stress-mediated mitochondrial dysfunction, we
320 knocked down ATF4 expression using ATF4 siRNA and found a significant knockdown of ATF4 after chronic ER
321 stress. ATF4 is recognized for its role as a protective factor during cellular stress. Its pro-death function has been
322 linked to its regulation of CHOP, which is involved in triggering apoptosis in response to ER stress.[28,29] We
323 observed decreased expression of ATF4, CHOP along with other caspases (cleaved cas 3 and 9) under ATF4
324 siRNA compared to control siRNA after Tun, suggesting ATF4 knockdown rescues the cell death-related

325 molecules after chronic ER stress (**Fig. 4A**). We also focused on mitophagy contributing protein, Mfn2, a
326 mitochondrial fusion protein, which plays a crucial role in regulating mitochondrial dynamics following stress. We
327 also investigated another mitophagy contributing protein, Tim23, which is an integral inner membrane protein
328 essential for mitochondrial import. [30] Tim23 depletion from cells results in a defect in import.[31] Mfn2 and Tim 23
329 increased in ATF4 siRNA compared to control siRNA after Tun **(Fig. 4A).** This data demonstrates that ATF4
330 regulates mitophagy-regulating molecules, possibly contributing to apoptosis. Parkin and PINK1 are key
331 regulators that control mitophagy and maintain mitochondrial homeostasis.[32] PINK1/Parkin-mediated mitophagy
332 is typically viewed in the context of mitochondrial depolarization by facilitating the turnover of damaged
333 mitochondria. We also investigated mitophagy initiator proteins (PINK1 and Parkin) and found that PINK1 levels
334 decreased and Parkin levels increased under ATF4 siRNA compared to control siRNA after tun treatment **(Fig.
335 4A).** This data suggests that ATF4 activation under chronic ER stress mediates the initiation of the Parkin-PINK1
336 mitophagy pathway. Mitophagy is typically initiated following the loss of MMP and mitochondrial fragmentation
337 in response to chronic stress. Thus, we determined MMP and found that the loss of MMP upon chronic ER stress
338 was rescued after ATF4 knockdown under Tun **(Fig. 4B).** Cell viability significantly increased under ATF4 siRNA
339 compared to control siRNA after Tun, as shown by MTT assay **(Fig. 4C).** The immunostaining data in primary
340 corneal endothelium cells showed that ATF4 gets induced and translocates to fragmented mitochondria after
341 Tunicamycin (also shown in **Fig 3I,J**) and ATF4 knockdown significantly decreased fragmented mitochondria
342 compared to control siRNA after tun **(Fig. 4D, E).** These data suggest that ATF4 regulates mitochondrial
343 dysfunction, contributing to CEnC apoptosis under chronic ER stress.

344 **ATF4 knockdown augments the mitophagy process despite a decrease in mitophagy-initiators under
345 chronic ER stress, thereby contributing to CEnC viability**

346 To determine whether mitophagy initiators are affected in the mitochondrial fraction under ATF4 manipulation
347 after chronic ER stress, we knock down ATF4, induce chronic ER stress, isolate mitochondria from 21T cells,
348 and probe for Parkin, PINK1, and LC3II. We found that Parkin and LC3II were upregulated, while PINK1 was
349 downregulated, in Tun-treated cells compared to DMSO-treated cells under control siRNA, suggesting chronic
350 ER stress mediates activation of mitophagy initiators. **(Fig. 5A).** When we knocked down ATF4, Parkin and LC3B
351 were downregulated, suggesting inhibition of mitophagy initiators. This finding led us to suspect that mitophagy
352 is inhibited after ATF4 knockdown under chronic ER stress, which could be detrimental to the cells, given that

353 many diseases involve mitophagy inhibition contributing to the loss of cell viability. However, this is not observed
354 in our data, as ATF4 knockdown increases cell viability after chronic ER stress (Fig. 4C). This suggests that even
355 though mitophagy initiators (Parkin, LCII) are inhibited under ATF4 knockdown after chronic ER stress, however,
356 the existing level of mitophagy initiators might be enough to complete the whole mitophagy process where we
357 should not see accumulation of damaged mitochondria in mitophagosomes. Therefore, we performed TEM and
358 analyzed mitophagosomes in ATF4 and control siRNA-treated 21T under DMSO and Tun conditions. Our TEM
359 data suggests a significant increase in mitophagosomes under Tunicamycin compared to DSMO under control
360 siRNA **(Fig. 5B, C).** This suggests that mitophagy is inhibited under chronic ER stress induced by Tun. ATF4
361 knockdown significantly decreases the number of mitophagosomes compared to control siRNA after tunicamycin
362 treatment **(Fig. 5B, C),** suggesting that ATF4 induction under chronic stress inhibits mitophagy, which may
363 contribute to the loss of cellular viability.

364 **ATF4$^{+/-}$ mice have significantly decreased CHOP activation and increased corneal endothelial cell**
365 **number compared to ATF4 $^{+/+}$ mice post-UVA**

366 We used our established UVA-induced mouse model of Fuchs' dystrophy[22] to investigate the loss of corneal
367 endothelial cells in *ATF4*$^{+/+}$ and *ATF4*$^{+/-}$ mice corneas. For this, we irradiated *ATF4* $^{+/+}$ and *ATF4* $^{+/-}$ mice' eyes
368 with UVA (200 J/cm^2) and observed the change in morphology of corneal endothelial (CE) cells, as outlined by
369 ZO-1 immunostaining, and counted the number of mouse CE cells. We found that *ATF4*$^{+/-}$ mice corneas have a
370 significantly increased number of corneal endothelial cells with more hexagonal morphology compared to *ATF4*
371 $^{+/+}$ mice post-UVA (**Fig. 6A, B**), which suggested ATF4 regulation of CE cell viability *in vivo*. To investigate whether
372 the increased CE cell number in ATF4+/- mice also results in decreased CHOP, a pro-apoptotic ER stress
373 molecule, we calculated the percentage of CE cells with CHOP activation. We found a significantly increased %
374 of CE cells with CHOP in *ATF4*$^{+/+}$ compared to *ATF4*$^{+/-}$ mice at day 1 post-UVA, with no differences in non-UVA
375 control (**Fig. 6C, D**). This suggests that ATF4 regulates CE cell viability by regulating CHOP activation *in vivo*.

376 **DISCUSSION**

377 ER stress and mitochondrial dysfunction have been known to independently contribute to CEnC apoptosis in
378 FECD. Our study reported that tun induces ER stress, which has been supported by numerous studies related
379 to ocular and neurodegenerative diseases.[5,33,34] In this study, we also investigated the differential induction of

380 pro-apoptotic ER stress and mitochondrial dysfunction in HCEnC-21T and F35T cell lines under unstressed
381 conditions and following tunicamycin. We specifically investigated the role of ATF4 in the PERK-ATF4-CHOP ER
382 stress pathway in mitochondrial dysfunction, mitophagy, and apoptosis in FECD. We demonstrated the
383 upregulation of a well-known ER stress pathway (eIF2α/ATF4/CHOP) in Fuchs' (F35T) compared to 21T cell
384 lines after Tunicamycin. This is supported by similar findings in many ocular diseases[35-37], where the higher
385 upregulation of the PERK-ATF4-CHOP ER stress pathway makes cells susceptible to apoptosis. Moreover, in
386 our previous publication, we demonstrated the increasing trend of ATF4 and CHOP in F35T compared to 21T at
387 the baseline. This is supported by similar findings here, where we observe a significant increase in ATF4 and a
388 trend towards increased CHOP levels in F35T compared to 21T under control (DMSO) conditions. A significantly
389 higher level of ATF4 in F35T cell line compared to 21T possibly makes them susceptible to apoptosis, specifically
390 to mitochondrial-mediated apoptosis. This hypothesis is supported by our findings of increased caspase-
391 mediated apoptotic molecules along with mitochondria-mediated apoptosis (Cleaved caspase 9, Bcl-2) in F35T
392 compared to 21T at baseline, which are further upregulated after chronic ER stress. We have not investigated
393 other models of apoptosis, such as ferroptosis under ER or mitochondrial stress in CEnCs, which will be
394 considered in the future.

395 Activation of mitochondrial-mediated apoptosis is reported to reduce MMP and ATP production and increase
396 mitochondrial fragmentation under pathological conditions. We have observed similar mitochondrial dysfunction
397 where we have increased mitochondrial fragmentation with low ATP and MMP in F35T compared to 21T cell line.
398 Mitochondrial fragmentation and MMP loss are further increased, along with reduced ATP in F35T compared to
399 21T after tunicamycin. Mitochondrial damage typically triggers mitophagy, which eliminates damaged
400 mitochondria under pathological conditions. PINK1/Parkin-mediated mitophagy is reported in Fuchs's with
401 activation of Parkin and LC3 and downregulation of PINK1. Our findings support this data, where we first see a
402 significant increase in the expression of Parkin and LC3 in F35T compared to 21T at baseline, suggesting
403 inherent mitochondrial damage in F35T and potentially contributing to its unhealthy state. Additionally, the
404 addition of tunicamycin increased Parkin and LC3 expressions in 21T but not in F35T cell lines. This suggests
405 that the F35T cell line, which is already sick under non-stress conditions, has already activated sufficient
406 mitophagy-initiator molecules. Thus, there is no further effect on mitophagy activation after chronic ER stress, at
407 least in the F35 T cell line. We will explore the effect of chronic ER stress on mitophagy mediators in other Fuchs

408 cell lines in the future. It is also possible that we may need to use either acute ER stress or analyze mitophagy
409 activation at an earlier time point (6 hours), which will help us understand the effect of mitophagy in this F35T
410 Fuchs' cell line. We will explore the effect of chronic ER stress on mitophagy mediators in less sick Fuchs cell
411 lines with fewer intronic repeats in the future. With respect to PINK1, our data demonstrates significantly
412 decreased expression of PINK1 in the F53T cell line compared to the 21T cell line under non-stress control, as
413 well as in response to Tunicamycin. This finding is consistent with our previous report, which demonstrated
414 downregulation of PINK1 along with upregulation of Parkin at a specific time point after chronic oxidative stress.[38]
415 In most cases, PINK1 activates Parkin, which tags/ubiquitinates damaged mitochondria for mitophagy. However,
416 there is PINK1-independent activation of Parkin for the initiation of mitophagy,[39] which could be the case under
417 chronic ER stress and will be investigated in the future.

418 ATF4 knockdown, either following tunicamycin in vitro or after UVA in vivo, decreased the pro-apoptotic ER stress
419 marker CHOP and reduced cellular apoptosis. These findings are supported by many studies under pathological
420 conditions.[35,40,41] Our data also demonstrate that ATF4 knockdown reduces MMP loss and mitochondrial
421 fragmentation in 21T after chronic ER stress. Similar studies[16,42,43] have been reported regarding ATF4 in other
422 cell types under various forms of cellular stress. However, knowledge about the role of ATF4 in mitophagy
423 remains limited.[17] Even though PINK1/parkin-mediated mitophagy is reported in Fuchs.[38] In general, it remains
424 unclear whether mitophagy is detrimental or beneficial in FECD. Mitophagy initiates with the recruitment of
425 mitophagy mediators (Parkin, LC3) to damaged mitochondria to form mitophagosomes and culminates with the
426 formation of mitophagic vacuoles containing degraded mitochondria. Mitophagy is considered inhibited if there
427 is a significant accumulation of damaged mitochondria in the form of mitophagosomes.[24,25] In the late-stage
428 Fuchs disease tissues, a study reports an abundance of autophagosomes with degraded mitochondria, along
429 with activation of PINK1/Parkin[3], suggesting excessive activation of mitophagy. However, excessive mitophagy
430 has not been confirmed with additional experiments. In our study, although Parkin and LC3 were activated after
431 chronic ER stress in 21T and F35 cell lines, we observed an abundance of mitophagosomes containing damaged
432 mitochondria, suggesting an inhibition of mitophagy. This discrepancy could be because of a specific kind of
433 stress, i.e., ER stress, on a cell line. It is also possible that initial mitophagy mediators (Parkin, LC3) are activating
434 mitophagy. However, extensive mitochondrial damage caused by chronic stress in cell lines probably prevents
435 the completion of all mitophagy steps, resulting in the accumulation of damaged mitochondria in

436 mitophagosomes. We also observed loss of Mfn2 in 21T and F35T cell lines after chronic ER stress. Mfn2 loss
437 is known to inhibit mitophagy, leading to the accumulation of damaged mitochondria as mitophagosomes in
438 cardiac[24] and skeletal diseases.[25] There is a possibility that Mfn2 loss is associated with the inhibition of
439 mitophagy in both 21T and F35T cell lines after chronic stress, which may be detrimental to cellular viability. We
440 will explore the role of different stressors in mitophagy for Fuchs in the future.

441 A previous study revealed that the mitophagy initiator, parkin, is transcriptionally regulated by ATF4.[15] This finding
442 supports our data, which show that Parkin is activated after Tun treatment under control siRNA conditions. We
443 also reported loss of Parkin after ATF4 knockdown in 21T cell line after tun. Even though Parkin and LC3 are
444 downregulated under ATF4 knockdown after chronic ER stress, suggesting inhibition of mitophagy. We do not
445 observe extensive mitophagosomes, even though the mitophagy initiator Parkin was downregulated under ATF4
446 knockdown conditions after chronic ER stress, which suggests that mitophagy is very active in this condition.
447 This could be possible due to the rescue of Mfn2 loss under ATF4 knockdown after Tun-induced chronic ER
448 stress, as shown in our data since Mfn2 loss increases mitophagosome formation and inhibits mitophagy in
449 cardiac and skeleton tissues.[24,25] In the future, we will explore the role of either ATF4 downstream targets, such
450 as CHOP, or other ER stress pathways in mitophagy. Our mouse model of UVA-induced ER stress in FECD
451 demonstrated loss of corneal endothelial cells in $ATF4^{+/+}$ UVA-irradiated mice, while $ATF4^{+/-}$ mice showed rescue
452 of cell loss post-UVA irradiation. This suggested the role of ATF4 in regulating cell loss *in vivo* as well.

453 As described above, ER stress and mitochondrial dysfunction have been known to independently contribute to
454 CEnC apoptosis in FECD. However, the role of specific ER stress pathways in regulating mitochondrial
455 dysfunction and mitophagy, as well as their contribution to CEnC apoptosis, remains unknown. Our study
456 provides insight into the crosstalk between ER and mitochondria, as well as the mechanism of ATF4-mediated
457 mitophagy in FECD. One of the limitations of the study is that we need to understand the molecular mechanism
458 by which ATF4 disrupts mitochondria and activates mitophagy. Specifically, it is not clear how ATF4 regulates
459 Parkin to control mitophagy in FECD. It remains unclear whether PINK1 regulates Parkin to control mitophagy
460 in FECD. Moreover, it also remains unclear whether Parkin/PINK-mediated mitophagy pathways are regulated
461 differently under different intracellular stresses. We also need to test the mechanism of mitophagy in detail in
462 animal models of FECD. Other limitations of this study are: 1) F35T is a transformed cell line with upregulated
463 stress by virtue of the model in and of itself as a contributor to some signaling, 2) High-dose UVA mouse model

464 may induce guttae but there is no genetic background of FECD; there is a lack of specificity in this model,
465 particularly because this model's excessive exposure is associated with damage of other ocular structures in the
466 anterior segment and inflammation that can induce ER stress apart from genetic FECD disease.

467 In future studies, we will investigate the mechanisms underlying parkin-mediated mitophagy, which contributes
468 to mitochondrial dysfunction and cell loss in FECD. We will also attempt to knock down ATF4 in F35T cells, which
469 will provide more specificity to our model, suggesting ATF4 is involved in FECD. The findings of our study are
470 promising and warrant further testing in FECD animal models. We will also target ER and mitochondrial stress
471 proteins for drug screening and provide therapeutic intervention for ocular diseases such as FECD. In summary,
472 we demonstrate that ATF4 transcription factor plays a key role in ER stress response, which leads to
473 mitochondrial dysfunction and altered mitophagy, thereby causing corneal endothelial cell apoptosis in FECD.
474 By modulating ATF4, we found that ER and mitochondrial stress were alleviated, resulting in enhanced cell
475 survival in the corneal endothelium. This study highlights the role of ATF4 in regulating ER-mitochondrial
476 crosstalk in CEnC degeneration, contributing to FECD development.

477 ***Acknowledgments***

478 We sincerely thank Allison Sowa, Bill Janssen for electron microscopy processing and imaging at The
479 Microscopy CoRE, Icahn School of Medicine at Mount Sinai. We also thank Ula V. Jurkunas (Schepens Eye
480 Research Institute, Harvard University) for providing HCEnC-21T cell line and Albert Jun (Wilmer Eye Institute,
481 John Hopkins University) for providing F35T cell line.

482 ***Funding***

483 Supported by NIH/NEI (R00EY031339), Mount Sinai Seed Money, New York Eye and Ear Foundation, Sarah K
484 de Coizart Charitable Trust/Foundation awarded to V.K. and Challenge Grant from Research to Prevent
485 Blindness awarded to ophthalmology department.

486 **Disclosure: S.Qureshi**, None; **S.Y. Kim**, None; **S. Lee**, None; **L. Ritzer**, None; None; **W. Steidl**, None; **G.J.**
487 **Krest**, None; **A. Kasi**, None; **V. Kumar**, None.

References

1. Krachmer, J.H., Purcell, J.J., Jr., Young, C.W., and Bucher, K.D. (1978). Corneal endothelial dystrophy. A study of 64 families. Arch Ophthalmol *96*, 2036-2039. 10.1001/archopht.1978.03910060424004.
2. Poulsen, E.T., Dyrlund, T.F., Runager, K., Scavenius, C., Krogager, T.P., Hojrup, P., Thogersen, I.B., Sanggaard, K.W., Vorum, H., Hjortdal, J., and Enghild, J.J. (2014). Proteomics of Fuchs' endothelial corneal dystrophy support that the extracellular matrix of Descemet's membrane is disordered. J Proteome Res *13*, 4659-4667. 10.1021/pr500252r.
3. Benischke, A.S., Vasanth, S., Miyai, T., Katikireddy, K.R., White, T., Chen, Y., Halilovic, A., Price, M., Price, F., Jr., Liton, P.B., and Jurkunas, U.V. (2017). Activation of mitophagy leads to decline in Mfn2 and loss of mitochondrial mass in Fuchs endothelial corneal dystrophy. Sci Rep *7*, 6656. 10.1038/s41598-017-06523-2.
4. Halilovic, A., Schmedt, T., Benischke, A.S., Hamill, C., Chen, Y., Santos, J.H., and Jurkunas, U.V. (2016). Menadione-Induced DNA Damage Leads to Mitochondrial Dysfunction and Fragmentation During Rosette Formation in Fuchs Endothelial Corneal Dystrophy. Antioxid Redox Signal *24*, 1072-1083. 10.1089/ars.2015.6532.
5. Okumura, N., Kitahara, M., Okuda, H., Hashimoto, K., Ueda, E., Nakahara, M., Kinoshita, S., Young, R.D., Quantock, A.J., Tourtas, T., et al. (2017). Sustained Activation of the Unfolded Protein Response Induces Cell Death in Fuchs' Endothelial Corneal Dystrophy. Invest Ophthalmol Vis Sci *58*, 3697-3707. 10.1167/iovs.16-21023.
6. Okumura, N., Hashimoto, K., Kitahara, M., Okuda, H., Ueda, E., Watanabe, K., Nakahara, M., Sato, T., Kinoshita, S., Tourtas, T., et al. (2017). Activation of TGF-beta signaling induces cell death via the unfolded protein response in Fuchs endothelial corneal dystrophy. Sci Rep *7*, 6801. 10.1038/s41598-017-06924-3.
7. Kaur, S., Sehrawat, A., Mastana, S.S., Kandimalla, R., Sharma, P.K., Bhatti, G.K., and Bhatti, J.S. (2023). Targeting calcium homeostasis and impaired inter-organelle crosstalk as a potential therapeutic approach in Parkinson's disease. Life Sci *330*, 121995. 10.1016/j.lfs.2023.121995.

8. Naia, L., Ferreira, I.L., Ferreiro, E., and Rego, A.C. (2017). Mitochondrial Ca(2+) handling in Huntington's and Alzheimer's diseases - Role of ER-mitochondria crosstalk. Biochem Biophys Res Commun *483*, 1069-1077. 10.1016/j.bbrc.2016.07.122.

9. Sakai, S., Watanabe, S., Komine, O., Sobue, A., and Yamanaka, K. (2021). Novel reporters of mitochondria-associated membranes (MAM), MAMtrackers, demonstrate MAM disruption as a common pathological feature in amyotrophic lateral sclerosis. FASEB J *35*, e21688. 10.1096/fj.202100137R.

10. Wang, X., Luo, D., and Wu, S. (2021). Molecular Dysfunctions of Mitochondria-Associated Endoplasmic Reticulum Contacts in Atherosclerosis. Oxid Med Cell Longev *2021*, 2424509. 10.1155/2021/2424509.

11. Qureshi, S., Lee, S., Steidl, W., Ritzer, L., Parise, M., and Kumar, V. (2023). Endoplasmic reticulum stress disrupts mitochondrial bioenergetics and dynamics and causes corneal endothelial apoptosis in Fuchs Dystrophy. Investigative Ophthalmology & Visual Science *64*, 1330-1330.

12. Qureshi, S., Lee, S., Steidl, W., Ritzer, L., Parise, M., Chaubal, A., and Kumar, V. (2023). Endoplasmic Reticulum Stress Disrupts Mitochondrial Bioenergetics, Dynamics and Causes Corneal Endothelial Cell Apoptosis. Invest Ophthalmol Vis Sci *64*, 18. 10.1167/iovs.64.14.18.

13. Neill, G., and Masson, G.R. (2023). A stay of execution: ATF4 regulation and potential outcomes for the integrated stress response. Front Mol Neurosci *16*, 1112253. 10.3389/fnmol.2023.1112253.

14. Pakos-Zebrucka, K., Koryga, I., Mnich, K., Ljujic, M., Samali, A., and Gorman, A.M. (2016). The integrated stress response. EMBO Rep *17*, 1374-1395. 10.15252/embr.201642195.

15. Bouman, L., Schlierf, A., Lutz, A.K., Shan, J., Deinlein, A., Kast, J., Galehdar, Z., Palmisano, V., Patenge, N., Berg, D., et al. (2011). Parkin is transcriptionally regulated by ATF4: evidence for an interconnection between mitochondrial stress and ER stress. Cell Death Differ *18*, 769-782. 10.1038/cdd.2010.142.

16. Quiros, P.M., Prado, M.A., Zamboni, N., D'Amico, D., Williams, R.W., Finley, D., Gygi, S.P., and Auwerx, J. (2017). Multi-omics analysis identifies ATF4 as a key regulator of the mitochondrial stress response in mammals. J Cell Biol *216*, 2027-2045. 10.1083/jcb.201702058.

17. Dlamini, M.B., Gao, Z., Hasenbilige, Jiang, L., Geng, C., Li, Q., Shi, X., Liu, Y., and Cao, J. (2021). The crosstalk between mitochondrial dysfunction and endoplasmic reticulum stress promoted ATF4-

mediated mitophagy induced by hexavalent chromium. Environ Toxicol *36*, 1162-1172. 10.1002/tox.23115.

18. B'Chir, W., Maurin, A.C., Carraro, V., Averous, J., Jousse, C., Muranishi, Y., Parry, L., Stepien, G., Fafournoux, P., and Bruhat, A. (2013). The eIF2alpha/ATF4 pathway is essential for stress-induced autophagy gene expression. Nucleic Acids Res *41*, 7683-7699. 10.1093/nar/gkt563.
19. Luhr, M., Torgersen, M.L., Szalai, P., Hashim, A., Brech, A., Staerk, J., and Engedal, N. (2019). The kinase PERK and the transcription factor ATF4 play distinct and essential roles in autophagy resulting from tunicamycin-induced ER stress. J Biol Chem *294*, 8197-8217. 10.1074/jbc.RA118.002829.
20. Hiramatsu, N., Messah, C., Han, J., LaVail, M.M., Kaufman, R.J., and Lin, J.H. (2014). Translational and posttranslational regulation of XIAP by eIF2alpha and ATF4 promotes ER stress-induced cell death during the unfolded protein response. Mol Biol Cell *25*, 1411-1420. 10.1091/mbc.E13-11-0664.
21. Bahamondes Lorca, V.A., Bastidas Mayorga, B.D., Tong, L., and Wu, S. (2021). UVB-induced eIF2alpha phosphorylation in keratinocytes depends on decreased ATF4, GADD34 and CReP expression levels. Life Sci *286*, 120044. 10.1016/j.lfs.2021.120044.
22. Liu, C., Miyajima, T., Melangath, G., Miyai, T., Vasanth, S., Deshpande, N., Kumar, V., Ong Tone, S., Gupta, R., Zhu, S., et al. (2020). Ultraviolet A light induces DNA damage and estrogen-DNA adducts in Fuchs endothelial corneal dystrophy causing females to be more affected. Proc Natl Acad Sci U S A *117*, 573-583. 10.1073/pnas.1912546116.
23. Engler, C., Kelliher, C., Spitze, A.R., Speck, C.L., Eberhart, C.G., and Jun, A.S. (2010). Unfolded protein response in fuchs endothelial corneal dystrophy: a unifying pathogenic pathway? Am J Ophthalmol *149*, 194-202 e192. 10.1016/j.ajo.2009.09.009.
24. Zhao, T., Huang, X., Han, L., Wang, X., Cheng, H., Zhao, Y., Chen, Q., Chen, J., Cheng, H., Xiao, R., and Zheng, M. (2012). Central role of mitofusin 2 in autophagosome-lysosome fusion in cardiomyocytes. J Biol Chem *287*, 23615-23625. 10.1074/jbc.M112.379164.
25. Sebastian, D., Sorianello, E., Segales, J., Irazoki, A., Ruiz-Bonilla, V., Sala, D., Planet, E., Berenguer-Llergo, A., Munoz, J.P., Sanchez-Feutrie, M., et al. (2016). Mfn2 deficiency links age-related sarcopenia and impaired autophagy to activation of an adaptive mitophagy pathway. EMBO J *35*, 1677-1693. 10.15252/embj.201593084.

26. Fusakio, M.E., Willy, J.A., Wang, Y., Mirek, E.T., Al Baghdadi, R.J., Adams, C.M., Anthony, T.G., and Wek, R.C. (2016). Transcription factor ATF4 directs basal and stress-induced gene expression in the unfolded protein response and cholesterol metabolism in the liver. Mol Biol Cell *27*, 1536-1551. 10.1091/mbc.E16-01-0039.

27. Wu, D., and Liang, J. (2024). Activating transcription factor 4: a regulator of stress response in human cancers. Front Cell Dev Biol *12*, 1370012. 10.3389/fcell.2024.1370012.

28. Zinszner, H., Kuroda, M., Wang, X., Batchvarova, N., Lightfoot, R.T., Remotti, H., Stevens, J.L., and Ron, D. (1998). CHOP is implicated in programmed cell death in response to impaired function of the endoplasmic reticulum. Genes Dev *12*, 982-995. 10.1101/gad.12.7.982.

29. Armstrong, J.L., Flockhart, R., Veal, G.J., Lovat, P.E., and Redfern, C.P. (2010). Regulation of endoplasmic reticulum stress-induced cell death by ATF4 in neuroectodermal tumor cells. J Biol Chem *285*, 6091-6100. 10.1074/jbc.M109.014092.

30. Dekker, P.J., Martin, F., Maarse, A.C., Bomer, U., Muller, H., Guiard, B., Meijer, M., Rassow, J., and Pfanner, N. (1997). The Tim core complex defines the number of mitochondrial translocation contact sites and can hold arrested preproteins in the absence of matrix Hsp70-Tim44. EMBO J *16*, 5408-5419. 10.1093/emboj/16.17.5408.

31. Emtage, J.L., and Jensen, R.E. (1993). MAS6 encodes an essential inner membrane component of the yeast mitochondrial protein import pathway. J Cell Biol *122*, 1003-1012. 10.1083/jcb.122.5.1003.

32. Swerdlow, N.S., and Wilkins, H.M. (2020). Mitophagy and the Brain. Int J Mol Sci *21*. 10.3390/ijms21249661.

33. Oda, T., Kosuge, Y., Arakawa, M., Ishige, K., and Ito, Y. (2008). Distinct mechanism of cell death is responsible for tunicamycin-induced ER stress in SK-N-SH and SH-SY5Y cells. Neurosci Res *60*, 29-39. 10.1016/j.neures.2007.09.005.

34. Li, Y., Li, H.Y., Shao, J., Zhu, L., Xie, T.H., Cai, J., Wang, W., Cai, M.X., Wang, Z.L., Yao, Y., and Wei, T.T. (2022). GRP75 Modulates Endoplasmic Reticulum-Mitochondria Coupling and Accelerates Ca(2+)-Dependent Endothelial Cell Apoptosis in Diabetic Retinopathy. Biomolecules *12*. 10.3390/biom12121778.

35. Ying, Y., Xue, R., Yang, Y., Zhang, S.X., Xiao, H., Zhu, H., Li, J., Chen, G., Ye, Y., Yu, M., et al. (2021). Activation of ATF4 triggers trabecular meshwork cell dysfunction and apoptosis in POAG. Aging (Albany NY) *13*, 8628-8642. 10.18632/aging.202677.

36. Kasetti, R.B., Patel, P.D., Maddineni, P., Patil, S., Kiehlbauch, C., Millar, J.C., Searby, C.C., Raghunathan, V., Sheffield, V.C., and Zode, G.S. (2020). ATF4 leads to glaucoma by promoting protein synthesis and ER client protein load. Nat Commun *11*, 5594. 10.1038/s41467-020-19352-1.

37. Fang, F., Liu, P., Huang, H., Feng, X., Li, L., Sun, Y., Kaufman, R.J., and Hu, Y. (2023). RGC-specific ATF4 and/or CHOP deletion rescues glaucomatous neurodegeneration and visual function. Mol Ther Nucleic Acids *33*, 286-295. 10.1016/j.omtn.2023.07.015.

38. Miyai, T., Vasanth, S., Melangath, G., Deshpande, N., Kumar, V., Benischke, A.S., Chen, Y., Price, M.O., Price, F.W., Jr., and Jurkunas, U.V. (2019). Activation of PINK1-Parkin-Mediated Mitophagy Degrades Mitochondrial Quality Control Proteins in Fuchs Endothelial Corneal Dystrophy. Am J Pathol *189*, 2061-2076. 10.1016/j.ajpath.2019.06.012.

39. Kubli, D.A., Cortez, M.Q., Moyzis, A.G., Najor, R.H., Lee, Y., and Gustafsson, A.B. (2015). PINK1 Is Dispensable for Mitochondrial Recruitment of Parkin and Activation of Mitophagy in Cardiac Myocytes. PLoS One *10*, e0130707. 10.1371/journal.pone.0130707.

40. Matus, S., Lopez, E., Valenzuela, V., Nassif, M., and Hetz, C. (2013). Functional contribution of the transcription factor ATF4 to the pathogenesis of amyotrophic lateral sclerosis. PLoS One *8*, e66672. 10.1371/journal.pone.0066672.

41. Pitale, P.M., Gorbatyuk, O., and Gorbatyuk, M. (2017). Neurodegeneration: Keeping ATF4 on a Tight Leash. Front Cell Neurosci *11*, 410. 10.3389/fncel.2017.00410.

42. Jiang, D., Cui, H., Xie, N., Banerjee, S., Liu, R.M., Dai, H., Thannickal, V.J., and Liu, G. (2020). ATF4 Mediates Mitochondrial Unfolded Protein Response in Alveolar Epithelial Cells. Am J Respir Cell Mol Biol *63*, 478-489. 10.1165/rcmb.2020-0107OC.

43. Le, H.T., Yu, J., Ahn, H.S., Kim, M.J., Chae, I.G., Cho, H.N., Kim, J., Park, H.K., Kwon, H.N., Chae, H.J., et al. (2025). eIF2alpha phosphorylation-ATF4 axis-mediated transcriptional reprogramming mitigates mitochondrial impairment during ER stress. Mol Cells *48*, 100176. 10.1016/j.mocell.2024.100176.

Figure 1. Differential activation of ER stress markers after chronic ER stress in normal human corneal endothelium cell line (21T), Fuchs (F35T) cell line, primary human corneal endothelial cells, and human corneal tissues. (A) Representative Western blot data showing differential activation of ER stress-related proteins (eIF2α, p-eIF2α, CHOP, and ATF4) in 21T and F35T cell lines under DMSO (0.2%) and Tun (10 μg/mL) for 24 h; DMSO was used as solvent control. **(B)** Quantification of westen blots demonstrating increased expression of ATF4 and CHOP in F35T compared to 21T after Tun (n=3-5, **P < 0.01, ***P < 0.001,one-way ANOVA with Tukey's multiple comparison test). **(C)** Immunostaining images ATF4 (green) and mitochondria (labeled with mitotracker red) in F35T and 21T cell lines under normal physiological conditions. **(D)** Quantification of immunostaining data showing increased % of cells with ATF4 induction in F35T compared to 21T cell line under normal physiological conditions (n = 3, **P < 0.01, unpaired t-test). **(E)** Immunostaining images showing ATF4 activation after treatment with Tun (10 μg/mL, 24h) in primary human corneal endothelial cells. **(F)** Immunostaining showing ATF4 and CHOP induction after treatment with Tun (10 μg/mL, 24 h) in human corneal endothelial tissues. (scale bar: 40 μm for all immuno images).

Figure 2. Differential mitochondrial dysfunction induced by ER stress in 21T and F35T. (A) Bar graph demonstrating differential MMP loss between 21T and F35T cell lines with and without Tun treatment (0.01, 0.1, 1, and 10 μg/mL Tun) (n = 3, ***P < 0.001, ****P < 0.0001, one-way ANOVA with Tukey's multiple comparison test). **(B)** Bar graph demonstrating differences in ATP production between untreated and treated (10 μg/mL Tun) 21T and F35T cell lines; (n = 7, *P < 0.05, **P < 0.01, ***P < 0.001, ****P < 0.0001, one-way ANOVA with Tukey's multiple comparison test). **(C, D)** Representative immunostaining and quantification showing increased mitochondrial fragmentation (observed by diffuse cytochrome C staining and loss of mitochondrial tubular networks) in F35T compared to 21T cell line after Tun treatment (10 μg/mL at 24h). F35T cell line also has significantly increased mitochondrial fragmentation compared to 21T cell under DMSO control at 24 h (n = 4, *P < 0.05, ***P < 0.001, one-way ANOVA with Tukey's multiple comparison test, scale bar: 40 μm), **(E)** Representative Western blots showing differential activation of mitochondrial-mediated intrinsic apoptotic proteins. (Bcl2, Cleaved Cas9, Cleaved Cas3, and PARP) in 21T compared to F35T cell lines under physiological conditions. **(F)** Bar graph demonstrating increased activation of PARP, Cleaved cas 3,9 and decreased activation of anti-apoptotic protein, Bcl-2 in F35T cell line compared to 21T cell line under physiological conditions (n = 4, *P < 0.05, **P < 0.01, unpaired t-test). **(G)** Cleavage 3/7 activity assay showing significantly increased Cleaved

3/7 activity in F35T compared to 21T after Tun (10 µg/mL at 24h). **(H)** Representative western blot along with quantification showing increasing trend of cleaved caspase 3, but no change in Bcl-2 in F35T compared to 21T after DMSO (0.2%) and Tun (10 µg/mL at 24h) (n = 4, *P < 0.05, ***P < 0.001, one-way ANOVA with Tukey's multiple comparison test). Representative western blot and quantification showing increased expression of **(I)** cleaved PARP **(J)** caspase 9 in F35T compared to 21T after DMSO (0.2%) and Tun (10 µg/mL at 24h) (n = 4, *P < 0.05, ***P < 0.001, one-way ANOVA with Tukey's multiple comparison test, scale bar: 40 µm).

Figure 3. Altered mitophagy under chronic ER stress in 21T and F35T cell lines. (A) Representative western blots showing differential expression of Mfn2, LC3 I/II, PINK1, and Parkin in 21T and F35T cell lines under physiological conditions. **(B)** Bar graph demonstrating upregulation of parkin and LC3B, and downregulation of PINK1 and Mfn2 in F35T cell line compared to 21T cell line under normal conditions. Representative western blot and bar graph demonstrating **(C, D)** decreased expression of Mfn2 and increased expression of LC3 II/I in **(E, F)** increased expresssion of Parkin **(G,H)** decreased expresssion of PINK1 in F35T and 21T cell line under tun (10 µg/mL for 24 h). (n = 4-7, *P < 0.05, **P < 0.01, unpaired t-test for two groups and one-way ANOVA with Tukey's multiple comparison test for more than two groups). **(I)** Immunostained images showing increased parkin activation (green) and cytochrome C release (red) after treatment with Tun (20 µg/mL for 6 h) in 21T cell line (scale bar: 40 µm). **(J)** Quantification of immunostaining data showing % of fragmented mitochondria with Parkin induction post-Tun treatment (20 µg/mL for 6 h) compared to DMSO (n = 3, **P < 0.01, unpaired t-test). **(K)** TEM images showing swollen, fragmented mitochondria (denoted by #), along with a similar number of mitophagosomes (denoted by $), in F35T and 21T cell lines under treated conditions (10 µg/mL Tun for 24 h). Red-colored insets show enlarged images below for better visualization (scale bar: 1 µm).

Figure 4. ATF4 knockdown attenuates ER stress, MMP loss, mitophagy-mediator proteins, mitochondrial fragmentation, and apoptosis under chronic ER stress. (A) Western blots showing upregulation of pro-apoptotic ER stress proteins (ATF4, CHOP), downregulation of mitochondria mass related proteins (Mfn2, Tim23), upregulation of apoptotic proteins (cleaved caspase 3, cleaved caspase 9) and differential regulation of mitophagy mediator proteins (increaed Parkin and decreased PINK1) in Tun treated groups (10 µg/mL, 24h) compared to DMSO (0.2%, 24 h) under control siRNA and reversal of these ER, mitochondrial, mitophagy as well apoptosis proteins expression in ATF4-knockdown groups, compared to control siRNA under Tun. **(B)** Bar graph demonstrating MMP loss post Tun treatment (10 µg/mL Tun) comapred to DMSO (0.2%) under control

siRNA at 48 h in primary corneal endothelial cells while ATF4 knockdown rescues MMP loss compared to control siRNA under Tun **(C)** Bar graph demonstrating loss of cell viability using MTT post Tun treatment (10 µg/mL Tun) compared to DMSO (0.2%) under control siRNA and rescue of cell death post ATF4 siRNA treatment compared to control siRNA under Tun in primary corneal endothelial cells at 24 h; (For MMP and MTT, n = 3-4, *P < 0.05, ***P < 0.001, one-way ANOVA with Tukey's multiple comparison test). **(D)** Immunostaining for ATF4 (green) and cytochrome c (red), DAPI (blue) in primary human corneal endothelial cells for control and ATF4 siRNA under DMSO (0.2%) and Tun (10 µg/mL) at 24 h (scale bar: 40 µm). **(E)** Quantification of immunostaining data showing significant increase in % of fragmented mitochondria post tunicamycin treatment compared to DMSO under control siRNA and rescue of mitochondrial fragmentation after ATF4 siRNA comparfed to control siRNA under Tun (10 µg/mL Tun) (n = 5, *P < 0.05, **P < 0.01, one-way ANOVA with Tukey's multiple comparison test).

Figure 5. ATF4 knockdown decreases parkin-mediated mitophagy mediator proteins; however, it activates mitophagy under ER stress. (A) Western blot data from isolated mitochondrial fraction of 21T cells showing increased expression of ATF4, differential activation of mitophagy mediators (increased Parkin and LC3II and decreased PINK1) post ER stress (0.1 µg/mL Tun at 24 h) under control siRNA, and reversal of expression of mitophagy mediators under ATF4 siRNA compared to control siRNA post Tun. **(B)** TEM images showing mitochondria (denoted by $), mitophagosomes (denoted by #) under control siRNA and ATF4 siRNA with DMSO and Tun treatment (10 µg/mL) (C) Quantitive bar graph showing increased number of mitophagsomes in Tun condition compared to DMSO under control siRNA and a signiifcant decrease in number of mitophagosomes under ATF4 siRNA groups compared to control siRNA post Tun. (A total of 20-25 cells have been imaged using TEM for counting mitophagosomes, scale bar: 1 µm).

Figure 6. Genetic deletion of ATF4 decreases pro-apoptotic ER stress molecule, CHOP, and protects against UVA-induced cell death. (A) Representative Zonula occludens-1 (ZO-1, green) immunostaining showing enlargement and loss of corneal endothelial cells (CEnCs) in *ATF4+/+* compared to *ATF4+/-* mice at week 4 post-UVA (250 J/cm^2). **(B)** Bar graph representing a significant decrease in CEnC count in *ATF4+/+* compared to *ATF4+/-* mice post-UVA. **(C)** Representative immunostained images for CHOP (green) in *ATF4+/+* and *ATF4+/-* mice CEnCs at day 1 post-UVA. **(D)** Bar graph demonstrating a significant increase in % cells with

CHOP in *ATF4+/+* compared to *ATF4+/-* mice post-UVA (n = 5, **P < 0.01, ***P < 0.001, ****P < 0.0001 one-way ANOVA with Tukey's multiple comparison test) (UVA: 500J/cm^2, Scale bar: 40 μm).

Figure 1.

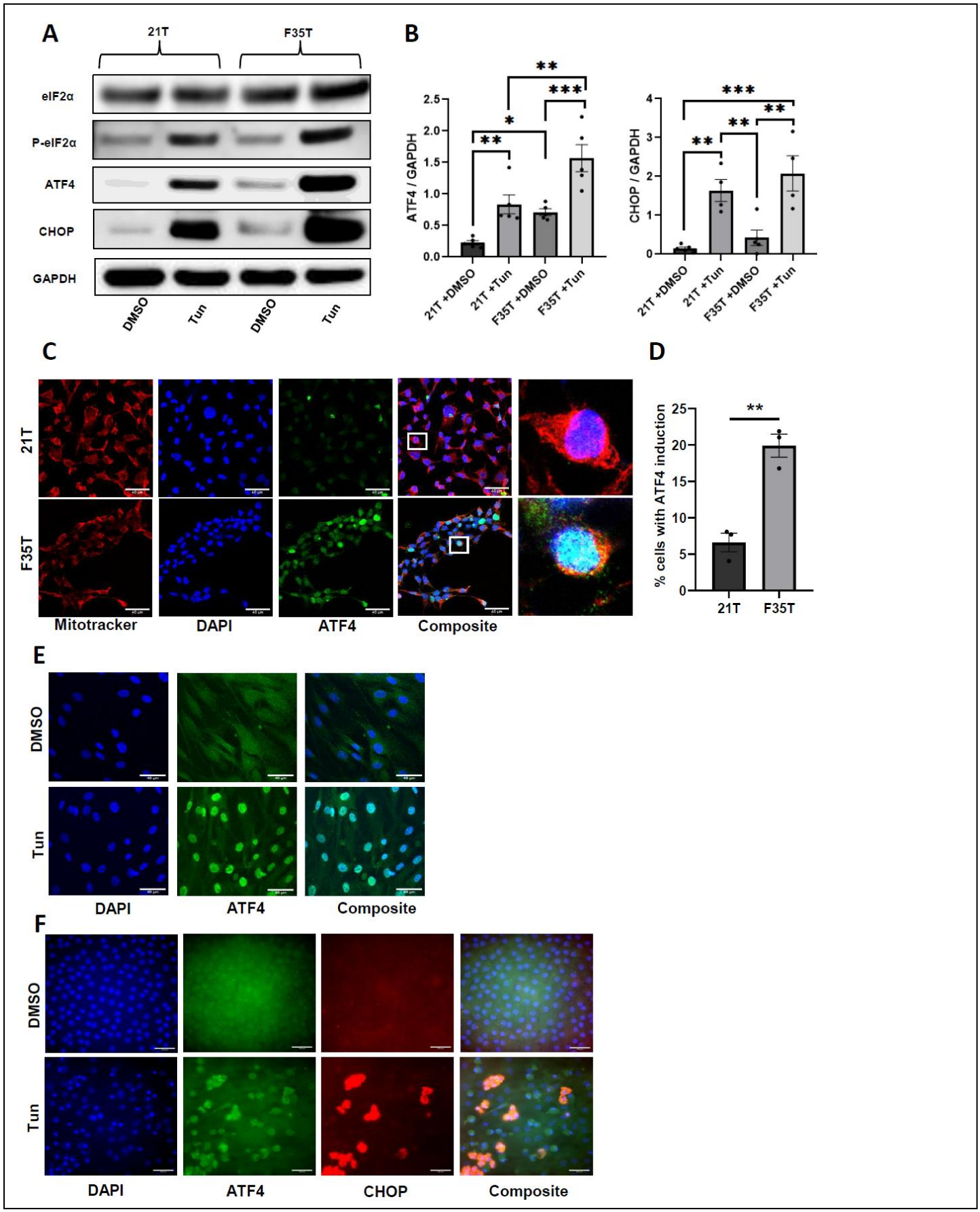
A
21T
F35T
eIF2α
P-eIF2α
ATF4
CHOP
GAPDH
DMSO
Tun
DMSO
Tun
B
ATF4 / GAPDH
CHOP / GAPDH
21T +DMSO
21T +Tun
F35T +DMSO
F35T +Tun
C
21T
F35T
Mitotracker
DAPI
ATF4
Composite
D
% cells with ATF4 induction
21T
F35T
E
DMSO
Tun
DAPI
ATF4
Composite
F
DMSO
Tun
DAPI
ATF4
CHOP
Composite

Figure 2.

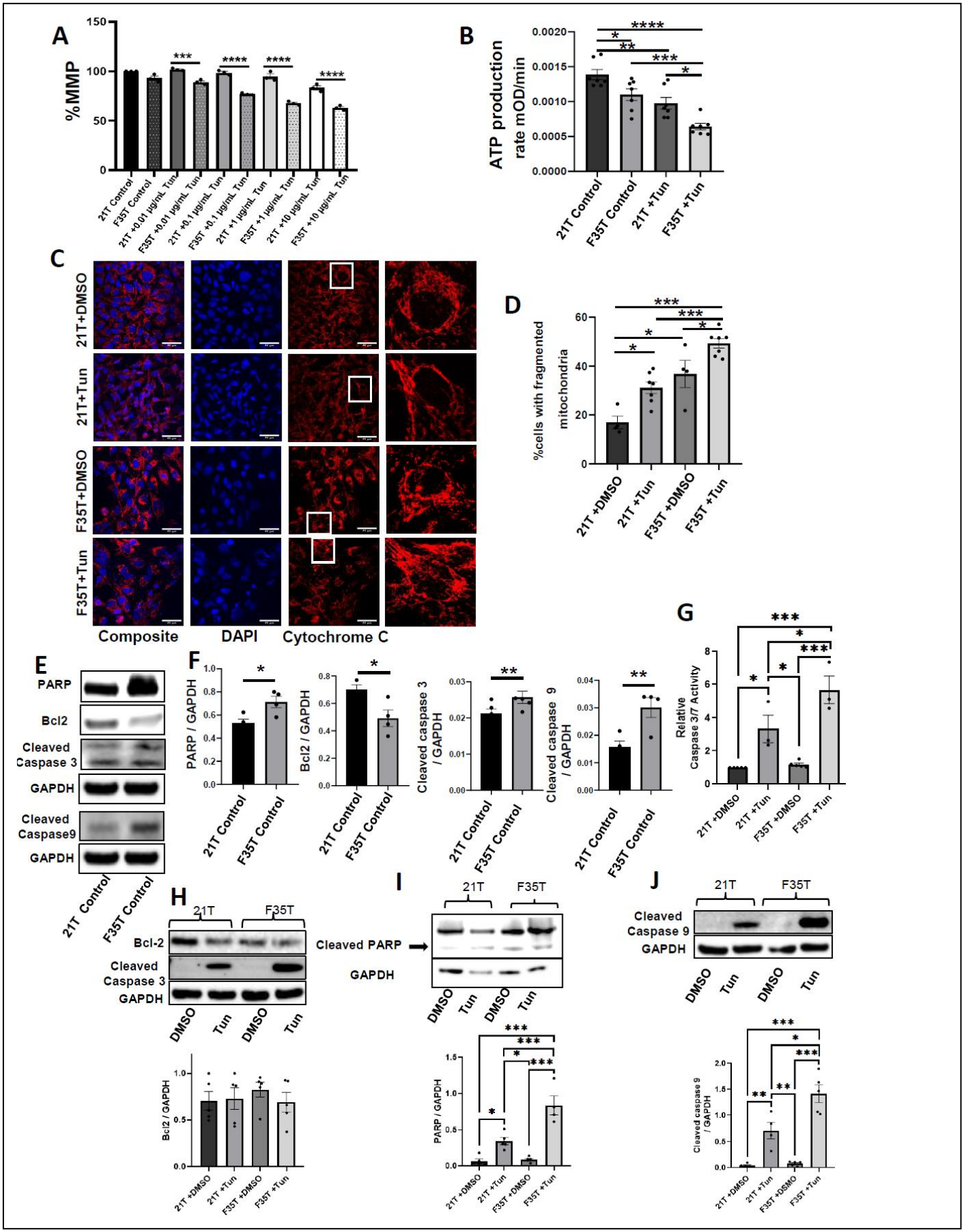
A
%MMP
21T Control
F35T Control
21T +0.01 µg/mL Tun
F35T +0.01 µg/mL Tun
21T +0.1 µg/mL Tun
F35T +0.1 µg/mL Tun
21T +1 µg/mL Tun
F35T +1 µg/mL Tun
21T +10 µg/mL Tun
F35T +10 µg/mL Tun
B
ATP production rate mOD/min
21T Control
F35T Control
21T +Tun
F35T +Tun
C
21T+DMSO
21T+Tun
F35T+DMSO
F35T+Tun
Composite
DAPI
Cytochrome C
D
%cells with fragmented mitochondria
21T +DMSO
21T +Tun
F35T +DMSO
F35T +Tun
E
PARP
Bcl2
Cleaved Caspase 3
GAPDH
Cleaved Caspase9
GAPDH
21T Control
F35T Control
F
PARP / GAPDH
Bcl2 / GAPDH
Cleaved caspase 3 / GAPDH
Cleaved caspase 9 / GAPDH
21T Control
F35T Control
G
Relative Caspase 3/7 Activity
21T +DMSO
21T +Tun
F35T +DMSO
F35T +Tun
H
21T
F35T
Bcl-2
Cleaved Caspase 3
GAPDH
DMSO
Tun
DMSO
Tun
Bcl2 / GAPDH
21T +DMSO
21T +Tun
F35T +DMSO
F35T +Tun
I
21T
F35T
Cleaved PARP
GAPDH
DMSO
Tun
DMSO
Tun
PARP / GAPDH
21T +DMSO
21T +Tun
F35T +DMSO
F35T +Tun
J
21T
F35T
Cleaved Caspase 9
GAPDH
DMSO
Tun
DMSO
Tun
Cleaved caspase 9 / GAPDH
21T +DMSO
21T +Tun
F35T +DSMO
F35T +Tun

Figure 3.

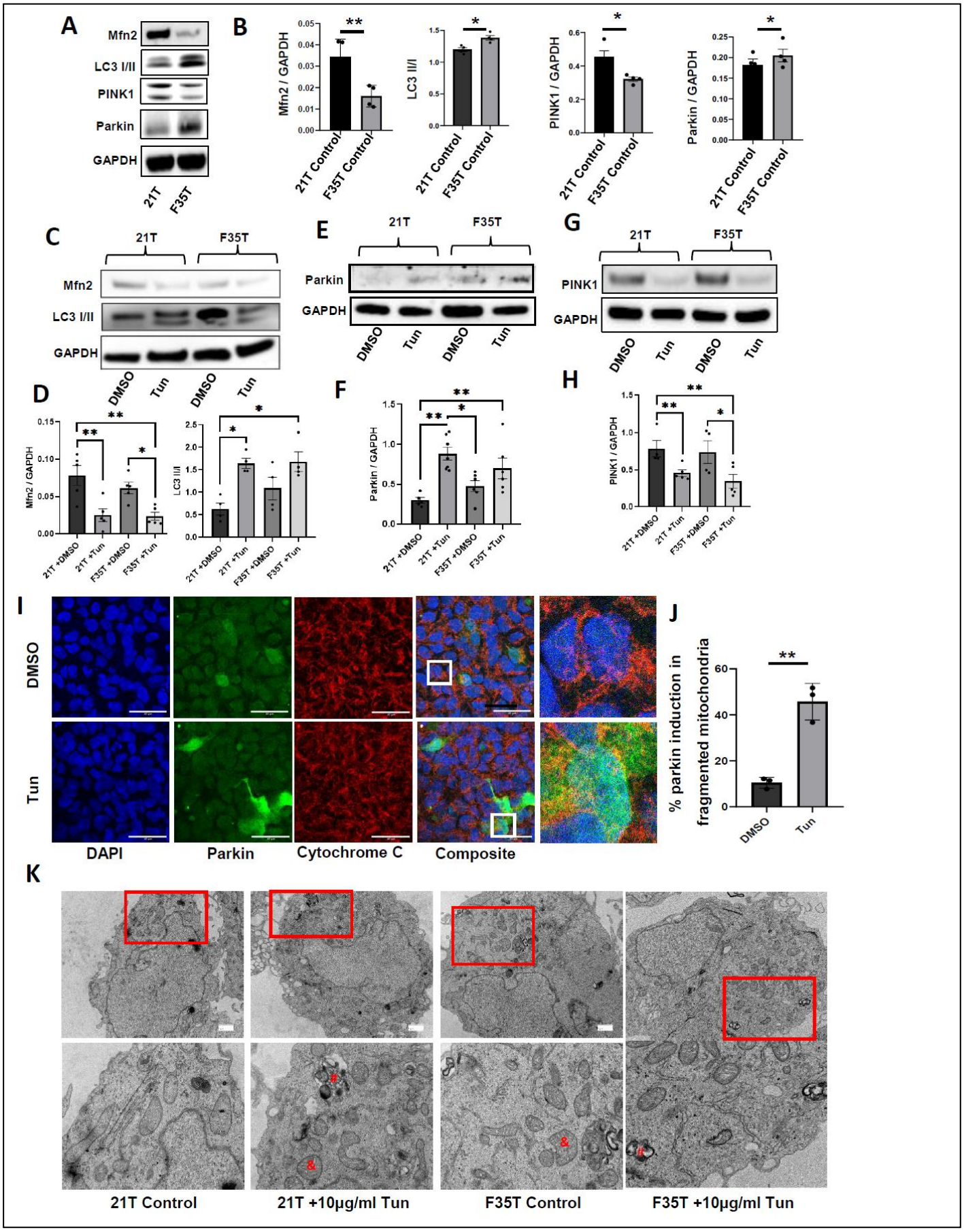
A
Mfn2
LC3 I/II
PINK1
Parkin
GAPDH
21T
F35T
B
Mfn2 / GAPDH
LC3 II/I
PINK1 / GAPDH
Parkin / GAPDH
21T Control
F35T Control
C
21T
F35T
Mfn2
LC3 I/II
GAPDH
DMSO
Tun
E
Parkin
G
PINK1
D
Mfn2 / GAPDH
LC3 II/I
21T +DMSO
21T +Tun
F35T +DMSO
F35T +Tun
F
Parkin / GAPDH
H
PINK1 / GAPDH
I
DMSO
Tun
DAPI
Parkin
Cytochrome C
Composite
J
% parkin induction in fragmented mitochondria
K
21T Control
21T +10μg/ml Tun
F35T Control
F35T +10μg/ml Tun

Figure 4.

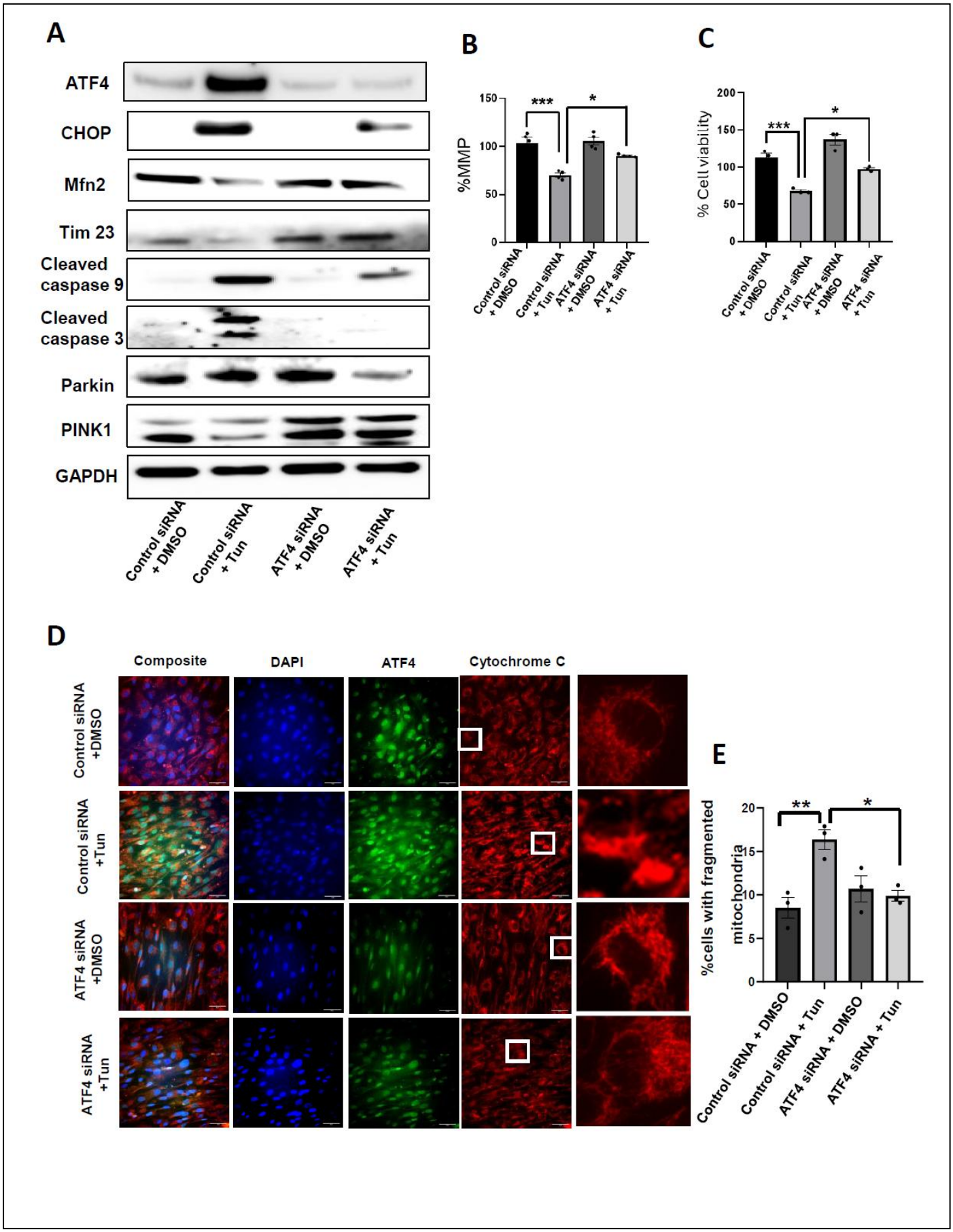
A
ATF4
CHOP
Mfn2
Tim 23
Cleaved caspase 9
Cleaved caspase 3
Parkin
PINK1
GAPDH
Control siRNA + DMSO
Control siRNA + Tun
ATF4 siRNA + DMSO
ATF4 siRNA + Tun
B
%MMP
150
100
50
0
***
*
C
% Cell viability
200
150
100
50
0
D
Composite
DAPI
ATF4
Cytochrome C
Control siRNA +DMSO
Control siRNA +Tun
ATF4 siRNA +DMSO
ATF4 siRNA +Tun
E
%cells with fragmented mitochondria
20
15
10
5
0
**
*

Figure 5.

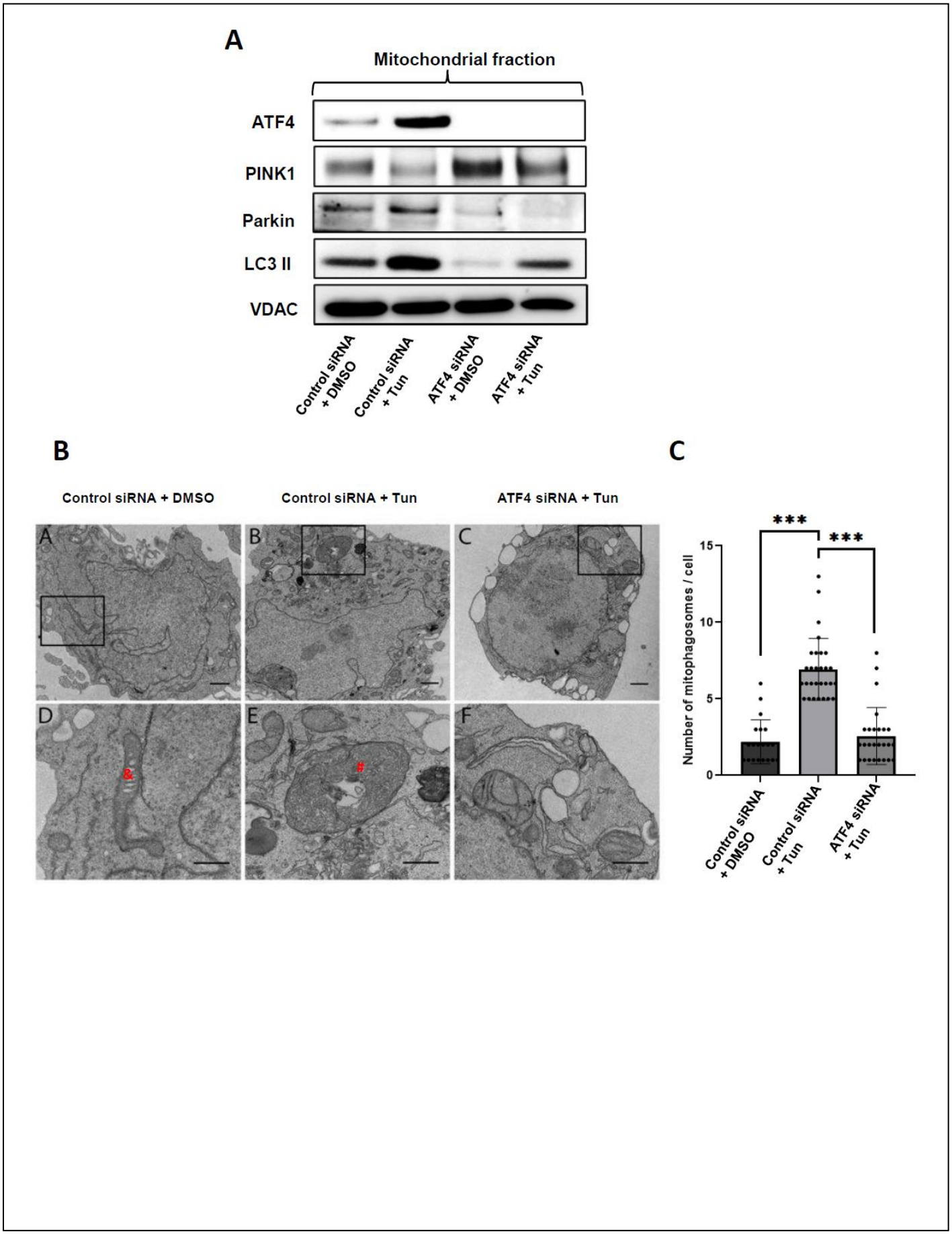
A
Mitochondrial fraction
ATF4
PINK1
Parkin
LC3 II
VDAC
Control siRNA + DMSO
Control siRNA + Tun
ATF4 siRNA + DMSO
ATF4 siRNA + Tun
B
Control siRNA + DMSO
Control siRNA + Tun
ATF4 siRNA + Tun
A
B
C
D
E
F
&
#
C
***
***
Number of mitophagosomes / cell
15
10
5
0
Control siRNA + DMSO
Control siRNA + Tun
ATF4 siRNA + Tun

Figure 6.

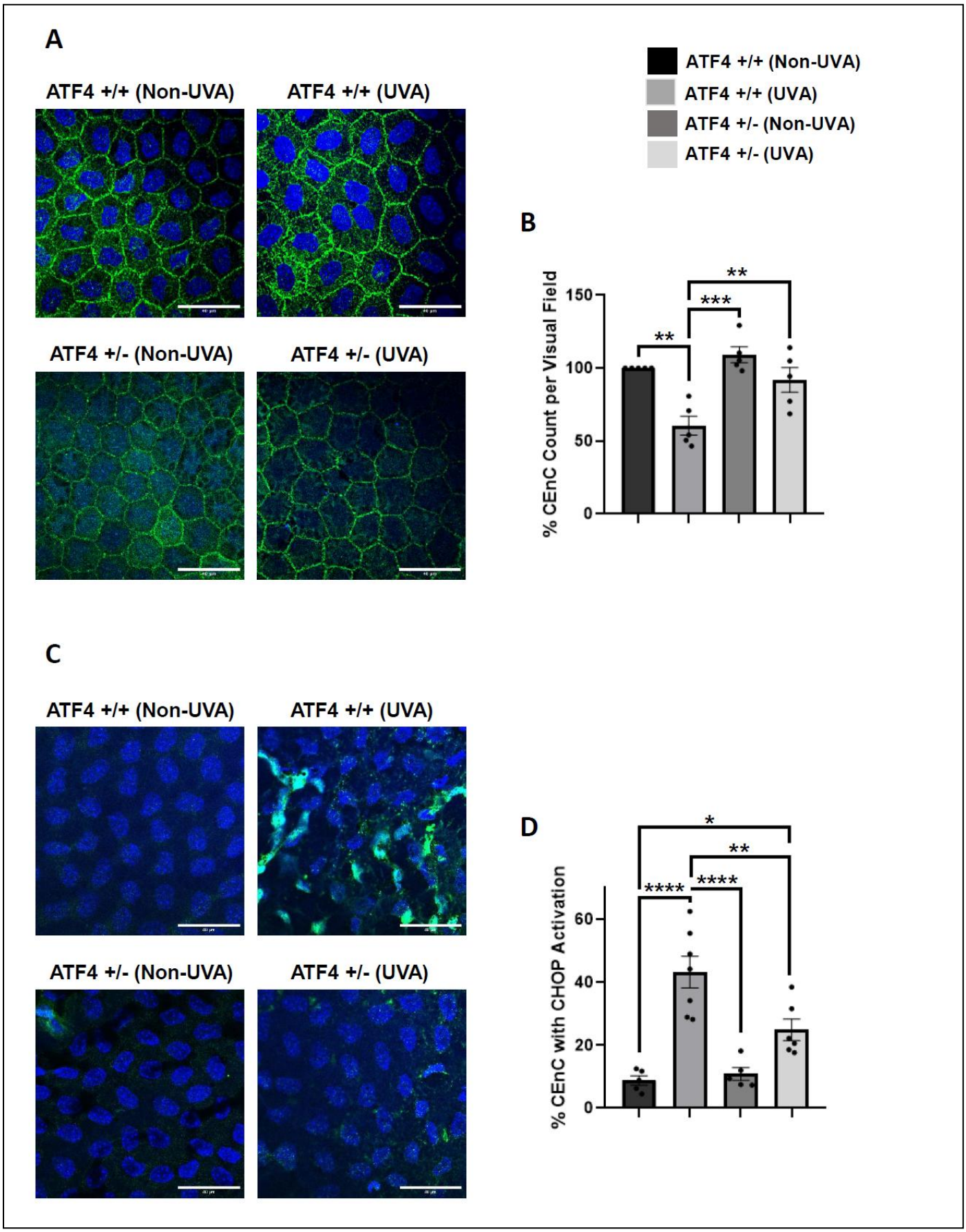
A
ATF4 +/+ (Non-UVA)
ATF4 +/+ (UVA)
ATF4 +/- (Non-UVA)
ATF4 +/- (UVA)
ATF4 +/+ (Non-UVA)
ATF4 +/+ (UVA)
ATF4 +/- (Non-UVA)
ATF4 +/- (UVA)
B
% CEnC Count per Visual Field
150
100
50
0
**
***
**
C
ATF4 +/+ (Non-UVA)
ATF4 +/+ (UVA)
ATF4 +/- (Non-UVA)
ATF4 +/- (UVA)
D
% CEnC with CHOP Activation
60
40
20
0
*
**
****
****